

Statistical features of quantum chaos using the Krylov operator complexity

Zhuoran Li and Wei Fan

Department of Physics, School of Science, Jiangsu University of Science and Technology, Zhenjiang, 212100, China

E-mail: zrl2l2r@gmail.com, fanwei@just.edu.cn

ABSTRACT: Recently the Krylov operator complexity is proposed to evaluate the operator growth in quantum systems, and the variance of its Lanczos coefficients is used as an important parameter for chaos. In this paper, we generate samples of random initial operators from given probability distributions (GOE, GUE and the uniform distribution). For the Sinai billiard model, we study the statistical properties of the variance of Lanczos coefficients in the associated Krylov space. Depending on whether the system is chaotic or not, the resulting distribution of the variance have different behaviors. In the nonchaotic case, the resulting distributions are almost overlapping together. In the chaotic case, they split into two well-separated groups. Besides, all the resulting distributions of the variance are the normal distribution, as long as the matrix size of the initial operator is large enough. This overlap-to-separation behavior, in the resulting distribution of the variance of Lanczos coefficients, may be a characteristics to distinguish chaotic and nonchaotic dynamics.

Contents

1	Introduction	1
2	Preliminary: Krylov operator space	2
3	Random initial Operators	4
4	Statistical properties of Lanczos coefficients	5
5	Model and Results	6
6	Discussion	10
A	Check the normal distribution of σ^2 for $\mathcal{N}_{max} = 100$	12
B	Different choice of algorithm step sizes for b_n	12
C	Check the normal distribution of σ^2 for $\mathcal{N}_{max} = 5$	14

1 Introduction

The physics of complexity is an important topic that contributes to our understanding of both classical and quantum chaos, especially the growth of operator complexity. Recently the Krylov complexity [1] is proposed as an upper bound on the operator complexity, including the famous bound $\lambda_L \leq 2\pi k_B T / \hbar$ [2] of the growth of the out-of-time-order correlation function (OTOC) [3]. The operator dynamics in the Krylov space resembles the hopping dynamics on the 1d chain [1]. From this, the connection between the dynamics of operator complexity and the Anderson localization is studied in [4], where the variance σ^2 of the Lanczos coefficients is connected to the late-time saturation of Krylov complexity.

Then a statistical correlation between the Krylov complexity and the level statistics [5–9] are firstly reported in spin systems [4, 10] and billiard systems [11]. For the billiard system [11], the variance of Lanczos coefficients is computed from the Krylov space of the momentum operator, and the level statistics are computed as usual. As the system Hamiltonian varies from nonchaotic to chaotic behavior, a sequence of data are generated for the level statistics and the variance of Lanczos coefficients. The statistical correlation coefficient between these two sequences of data are not zero. For the chaotic spin system [10], the late-time saturation of Krylov complexity approaches the behavior of Random Matrix Theory (RMT) under certain circumstances. Also, the operator generating the Krylov space is randomly selected and three different operators are compared [10]. Recently in [12], the Krylov complexity is studied by choosing multiple initial operators, instead of one single operator.

Along this line, it is a natural and straightforward question to ask what would happen if we do statistics on initial operators over a given probability distribution. In this paper, we study this possibility. We generate samples of initial operators from a probability distribution (GOE, GUE and the uniform distribution) and study the resulting distribution of the variance σ^2 of Lanczos coefficients. Interestingly, we find that for the nonchaotic case, the resulting distributions of the variance σ^2 are nearly the same for different distributions of initial operators. And surprisingly, for the chaotic case, the resulting distributions of the variance σ^2 are obviously different. *More intuitively, for different distributions of initial operators, the resulting plots of distributions are overlapped together in the nonchaotic case, and divide into two well-separated groups in the chaotic case.*

In detail, we consider a typical billiard system, the Sinai billiard, which originates from a quantization of classical chaos [13]. The computation is done in the energy representation and operators become matrices. For the random initial operator \mathcal{O} coming from the probability distribution GOE (GUE and the uniform distribution), the corresponding random matrix is sampled from the standard GOE (GUE and Hermitian matrices whose matrix elements follow the uniform distribution). Then the variance σ^2 of Lanczos coefficients is obtained in the associated Krylov space, when the system is chaotic or nonchaotic. By sampling the initial operator many times for each distribution, we can analyze the resulting statistical distribution of the variance σ^2 . We find that the resulting distribution of σ^2 is almost always the normal distribution, independent of the initial operator distribution. As the system changes from nonchaotic to chaotic, the resulting normal distributions of σ^2 is computed and the logarithm of its statistical average $\langle \sigma^2 \rangle$ and standard deviation are shown in Figure 5. In the nonchaotic case, the resulting distributions of σ^2 are almost overlapping together. In the chaotic case, they split into two groups well-separated from each other: one group consists of GOE, the uniform distribution of pure real numbers (URE) and of pure imaginary numbers (UIM), the other group is of GUE and the uniform distribution of complex numbers (UCP).

The paper is organized as follows. In Section 2, we briefly review the Krylov operator space. In Section 3, we explain the sampling of the random initial operator. In Section 4, we give a qualitative explanation for the reason why the resulting distribution of the variance σ^2 is always the normal distribution. In Section 5, we show the detailed results of the model-the Sinai billiard. In Section 6, we discuss the physics of our results and conclude with a discussion of open questions.

2 Preliminary: Krylov operator space

Here we briefly review the algorithms of Krylov operator space [1]. Readers familiar with it can skip this section. For a quantum system with the Hamiltonian H , the time evolution of a given operator \mathcal{O} in the Heisenberg picture is given by

$$\mathcal{O}(t) = e^{iHt}\mathcal{O}(0)e^{-iHt} \tag{2.1}$$

Using the Baker-Campbell-Hausdorff formula, it can be expanded as

$$\mathcal{O}(t) = \sum_{n=0}^{\infty} \frac{(it)^n}{n!} \mathcal{L}^n \mathcal{O}(0), \quad (2.2)$$

where $\mathcal{L} := [H, \cdot]$ is the Liouvillian superoperator. This sequence of operators $\mathcal{O}(0), \mathcal{L}\mathcal{O}(0), \mathcal{L}^2\mathcal{O}(0), \dots$ spans a space associated with the operator $\mathcal{O}(t)$. This space is the Krylov subspace generated by \mathcal{L} (and hence H) and $\mathcal{O}(0)$, that is,

$$\mathcal{K}_m(\mathcal{L}, \mathcal{O}(0)) \equiv \{\mathcal{O}(0), \mathcal{L}\mathcal{O}(0), \mathcal{L}^2\mathcal{O}(0), \dots, \mathcal{L}^m\mathcal{O}(0)\} \quad (2.3)$$

An orthonormal basis, called the Krylov basis, can be constructed for $\mathcal{K}_m(\mathcal{L}, \mathcal{O}(0))$. This construction also generates a sequence of important numbers called the Lanczos coefficients, because the algorithm used is the Lanczos algorithm (or similar algorithms). The orthogonality is guaranteed by the inner product $(A|B) = \text{tr}[A^\dagger B]$, which can be considered as a simplification of the Wightman inner product at infinite temperature. The Lanczos algorithm can be briefly stated as following:

Require: $\|\mathcal{O}\| = \sqrt{(\mathcal{O}|\mathcal{O})}$

- 1: $b_0 \leftarrow 0$
- 2: $\mathcal{O}_{-1} \leftarrow 0$
- 3: $\mathcal{O}_0 \leftarrow \mathcal{O}(0)/\|\mathcal{O}(0)\|$
- 4: $n \leftarrow 1$
- 5: **while** $b_n \neq 0$ **do**
- 6: $\mathcal{A}_n \leftarrow \mathcal{L}\mathcal{O}_{n-1} - b_{n-1}\mathcal{O}_{n-2}$
- 7: $b_n \leftarrow \|\mathcal{A}_n\|$
- 8: $\mathcal{O}_n \leftarrow \mathcal{A}_n/b_n$
- 9: $n \leftarrow n + 1$
- 10: **end while**

The Krylov basis is given by $\{|O_0\rangle, |O_1\rangle, \dots, |O_{n_k}\rangle\}$ and the dimension of Krylov operator space is $n_k = \dim(\mathcal{K}_m) - 1$. The sequence of positive numbers $\{b_n\}$ is called the Lanczos coefficient and is essentially the matrix element

$$L_{nm} \equiv (\mathcal{O}_n|\mathcal{L}|\mathcal{O}_m) = \begin{pmatrix} 0 & b_1 & 0 & 0 & \dots \\ b_1 & 0 & b_2 & 0 & \dots \\ 0 & b_2 & 0 & b_3 & \dots \\ 0 & 0 & b_3 & 0 & \ddots \\ \vdots & \vdots & \vdots & \ddots & \ddots \end{pmatrix} \quad (2.4)$$

The Lanczos coefficient $\{b_n\}$ contains all the information about the evolution of the operator. To see this, firstly expand the operator $\mathcal{O}(t)$ in terms of the Krylov basis

$$\mathcal{O}(t) = \sum_{n=0}^{n_k-1} i^n \varphi_n(t) \mathcal{O}_n, \quad \varphi_n(t) \equiv (\mathcal{O}_n|\mathcal{O}(t))/i^n, \quad (2.5)$$

and then substitute it into the Heisenberg equation. This would give

$$\dot{\varphi}_n(t) = b_n \varphi_{n-1}(t) - b_{n+1} \varphi_{n+1}(t), \quad (2.6)$$

where the dot is the time derivative and the initial condition is $\varphi_n(0) = \delta_{n0} \|O\|$. The logarithmic variance σ of the Lanczos coefficient $\{b_n\}$ is defined by

$$\sigma^2 := \text{Var}(x_i) = \langle x^2 \rangle - \langle x \rangle^2, x_i = \ln \frac{b_{2i-1}}{b_{2i}}. \quad (2.7)$$

In [1], the equation (2.6) is interpreted as the dynamics on a 1d chain, with $\varphi_n(t)$ being the wave function and b_n being hopping amplitude. Then the Krylov space can be associated with systems of spin chains. In this analog, the connection between the dynamics of complexity and the Anderson localization is studied in [4], and the importance of the variance of Lanczos coefficient is recognized.

3 Random initial Operators

In this paper, we choose samples of random initial operators from different probability distributions and study the resulting distribution of the variance σ^2 of the Lanczos coefficients. Specifically, we consider random initial operators (\mathcal{O}_{GOE} , \mathcal{O}_{GUE} and \mathcal{O}_{uni}) from the Gaussian orthogonal ensemble (GOE), the Gaussian unitary ensemble (GUE) and the uniform distribution.

These operators are evaluated in the energy representation. In the case of GOE, the random matrix, $\mathcal{O}_{mn} := \langle m | \mathcal{O}_{GOE} | n \rangle$, is a real symmetric matrix whose matrix elements satisfy the following joint probability density function [14]:

$$P(\mathcal{O}_{11}, \mathcal{O}_{12}, \dots, \mathcal{O}_{NN}) = \left(\frac{1}{2\pi}\right)^{\frac{N}{2}} \left(\frac{1}{\pi}\right)^{\frac{N^2-N}{2}} \exp\left[-\frac{1}{2}\text{Tr}(\mathcal{O}_{GOE}^2)\right]. \quad (3.1)$$

In the case of GUE, the random matrix, $\mathcal{O}_{mn}^{GUE} := \langle m | \mathcal{O}_{GUE} | n \rangle$ is Hermitian whose elements satisfy the following joint probability density function:

$$P\left(\mathcal{O}_{11}^{(0)}, \mathcal{O}_{12}^{(0)}, \dots, \mathcal{O}_{NN}^{(0)}\right) = \left(\frac{1}{2\pi}\right)^{\frac{N}{2}} \left(\frac{1}{\pi}\right)^{\frac{N^2-N}{2}} \exp\left[-\frac{1}{2}\text{Tr}(\mathcal{O}^{(0)2})\right] \quad (3.2)$$

$$P\left(\mathcal{O}_{11}^{(1)}, \mathcal{O}_{12}^{(1)}, \dots, \mathcal{O}_{NN}^{(1)}\right) = \left(\frac{1}{2\pi}\right)^{\frac{N}{2}} \left(\frac{1}{\pi}\right)^{\frac{N^2-N}{2}} \exp\left[-\frac{1}{2}\text{Tr}(\mathcal{O}^{(1)2})\right] \quad (3.3)$$

with $\mathcal{O}^{(0)}$ being the real part of \mathcal{O}_{mn}^{GUE} , and $\mathcal{O}^{(1)}$ being the imaginary part of \mathcal{O}_{mn}^{GUE} . In the case of uniform distribution, three types of random operators are studied. Their random matrices belong to three types: purely real symmetric (URE), purely imaginary Hermitian (UIM), and complex Hermitian (UCP).

For convenience, we introduce the distribution function $f_{\sigma^2}(\mathcal{O})$, whose value is the variance σ^2 of the Lanczos coefficients generated by the Krylov subspace $\mathcal{K}_m(\mathcal{L}, \mathcal{O})$ of the initial operator \mathcal{O}

$$f_{\sigma^2}(\mathcal{O}) := \text{the variance } \sigma^2 \text{ of Lanczos coefficients of the Krylov subspace } \mathcal{K}_m(\mathcal{L}, \mathcal{O}). \quad (3.4)$$

Obviously, the resulting distribution function f_{σ^2} depends on the initial distribution of the operator \mathcal{O} . Interestingly, when compare different initial probability distributions of \mathcal{O} , the behavior of the resulting distribution function f_{σ^2} depends on whether the system is nonchaotic or chaotic: nearly complete overlapping f_{σ^2} in the nonchaotic case, and two well-separated groups of f_{σ^2} in the chaotic case. For all cases, the distribution function f_{σ^2} is a normal distribution.

4 Statistical properties of Lanczos coefficients

Before showing detailed results, we give a qualitative analysis of the reason why the resulting distributions are normal distributions. This is related with the nature of the Krylov algorithm itself and can be understood using the central limit theorem of probability theory, so we explain it here in this section.

Firstly, we prove the following lemma by mathematical induction, which essentially says that the matrices involved in the Krylov algorithm depends only on the energy levels and the initial random matrix.

Lemma 1. *Matrix elements $\mathcal{O}_{mn}^{(k)}$ of Krylov basis \mathcal{O}_k in the energy representation can be written as:*

$$\mathcal{O}_{mn}^{(k)} = C_{mn}^{(k)}(b_1, b_2, \dots, b_k; E_{mn})\mathcal{O}_{mn}^{(0)} \quad (4.1)$$

where $E_{mn} := E_m - E_n$.

Proof. $k = 0, 1$ are clearly true, because

$$\mathcal{O}_{mn}^{(0)} = \mathcal{O}_{mn}^{(0)} \quad (4.2)$$

$$\mathcal{O}_{mn}^{(1)} = \frac{1}{b_1}\mathcal{A}_{mn}^{(1)} = \frac{1}{b_1}(E_{mn}\mathcal{O}_{mn}^{(0)}), b_1 = \|E_{mn}\mathcal{O}_{mn}^{(0)}\| \quad (4.3)$$

Assume that $k - 1, k - 2$ holds, then k also holds, because

$$\mathcal{A}_{mn}^{(k)} = E_{mn}\mathcal{O}_{mn}^{(k-1)} - b_{k-1}\mathcal{O}_{mn}^{(k-2)} \quad (4.4)$$

$$= [E_{mn}C_{mn}^{(k-1)}(b_1, b_2, \dots, b_{k-1}; E_{mn}) - b_{k-1}C_{mn}^{(k-2)}(b_1, b_2, \dots, b_{k-2}; E_{mn})]\mathcal{O}_{mn}^{(0)} \quad (4.5)$$

$$= \tilde{C}_{mn}^{(k)}(b_1, b_2, \dots, b_{k-1}; E_{mn})\mathcal{O}_{mn}^{(0)} \quad (4.6)$$

and

$$b_k = \|\tilde{C}_{mn}^{(k)}(b_1, b_2, \dots, b_{k-1}; E_{mn})\mathcal{O}_{mn}^{(0)}\| \quad (4.7)$$

$$\mathcal{O}_{mn}^{(k)} = \frac{1}{b_k}\mathcal{A}_{mn}^{(k)} = C_{mn}^{(k)}(b_1, b_2, \dots, b_k; E_{mn})\mathcal{O}_{mn}^{(0)}. \quad (4.8)$$

Then by mathematical induction the lemma is proved. \square

From this lemma, we see that all Lanczos coefficients $b_k = b_k(\mathcal{O}_{mn}^{(0)}; E_{mn})$ depend only on the energy levels and the initial random operator $\mathcal{O}_{mn}^{(0)}$. In practical computation, the energy levels are truncated to \mathcal{N}_{max} and the random matrix $\mathcal{O}_{mn}^{(0)}$ is of size $\mathcal{N}_{max} \times \mathcal{N}_{max}$.

If the value of \mathcal{N}_{max} is large, we would have large-enough random numbers, so qualitatively the resulting distribution can be estimated by the central limit theorem. This is one aspect related to the large value of \mathcal{N}_{max} .

In the other aspect, suppose the variance $\sigma_{\mathcal{O}}^2$ is computed from $2K$ Lanczos coefficients of a given initial operator $\mathcal{O}^{(0)}$, with $2K$ being the algorithm-steps selected from the Krylov space. By definition (2.7), we have

$$\begin{aligned}\sigma_{\mathcal{O}}^2 &= \frac{1}{K} \sum_{i=1}^K \left(x_i(\mathcal{O}^{(0)}; E_{mn}) \right)^2 - \frac{1}{K^2} \left(\sum_{i=1}^K x_i(\mathcal{O}^{(0)}; E_{mn}) \right)^2 \\ &= \left(\frac{1}{K} - \frac{1}{K^2} \right) \sum_{i=1}^K \left(x_i(\mathcal{O}^{(0)}; E_{mn}) \right)^2 - \frac{1}{K^2} \sum_{i \neq j} x_i(\mathcal{O}^{(0)}; E_{mn}) x_j(\mathcal{O}^{(0)}; E_{mn}).\end{aligned}\quad (4.9)$$

Qualitatively, we can expect that the second term with $i \neq j$ would be zero when averaging over initial operators $\mathcal{O}^{(0)}$. In one side, when the set size K of coefficients is large, the second term is already small compared with the first term. In the other side, when taking the average $\langle \cdot \rangle$ over the initial operators, we can expect

$$\sum_{i \neq j}^K \langle x_i(\mathcal{O}^{(0)}; E_{mn}) x_j(\mathcal{O}^{(0)}; E_{mn}) \rangle \sim \sum_{i \neq j}^K \langle x_i(\mathcal{O}^{(0)}; E_{mn}) \rangle \langle x_j(\mathcal{O}^{(0)}; E_{mn}) \rangle \sim 0. \quad (4.10)$$

This qualitatively can be understood from an analog with random walks and from the nature of the initial distribution (GOE, GUE and the uniform distribution). So after taking the average over initial random operators, we obtain qualitatively

$$\langle \sigma_{\mathcal{O}}^2 \rangle \sim \left(\frac{1}{K} - \frac{1}{K^2} \right) \sum_{i=1}^K \left\langle x_i(\mathcal{O}^{(0)}; E_{mn})^2 \right\rangle. \quad (4.11)$$

If the sample is large enough, we can qualitatively expect $\sigma_{\mathcal{O}}^2$ to follow the normal distribution as a result of the central limit theorem.

From the above qualitative analysis, we see that the numbers of random numbers are determined by \mathcal{N}_{max} , K and sample size of initial operators. If they are large enough, we would expect the resulting distribution to be normal. In the following computation, we use the choice $\mathcal{N}_{max} = 100$ and $K = 500$ in consistent with [11], and we average over 5000 initial operators. This number turns out to be large enough and the resulting distribution function f_{σ^2} is the normal distribution. (In Appendix C, we check the case $\mathcal{N}_{max} = 5$. The resulting distribution f_{σ^2} is not normal there, and interesting, the phenomenon of separation of f_{σ^2} for different initial distributions disappears.)

5 Model and Results

For concrete, we study the Sinai billiard which is a typical two-dimensional system of chaos. The Hamiltonian is defined by

$$H = p_x^2 + p_y^2 + V(x, y) \quad (5.1)$$

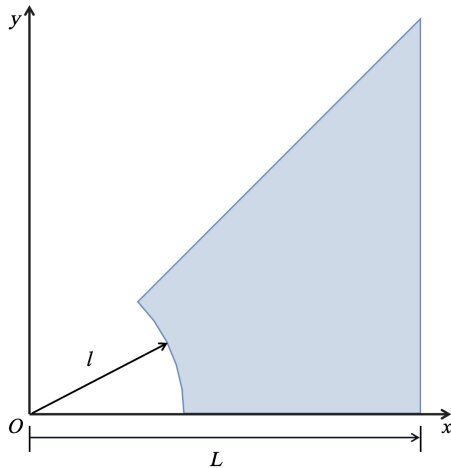


Figure 1: The region Ω of the potential (5.2) of the billiard. Dirichlet conditions are imposed on the boundaries.

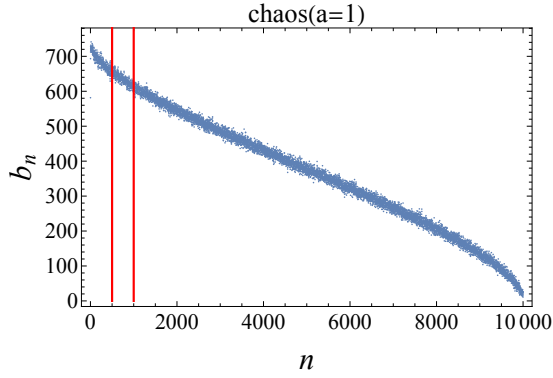
with the potential

$$V(x, y) = \begin{cases} 0 & (x, y) \in \Omega \\ \infty & \text{else} \end{cases}. \quad (5.2)$$

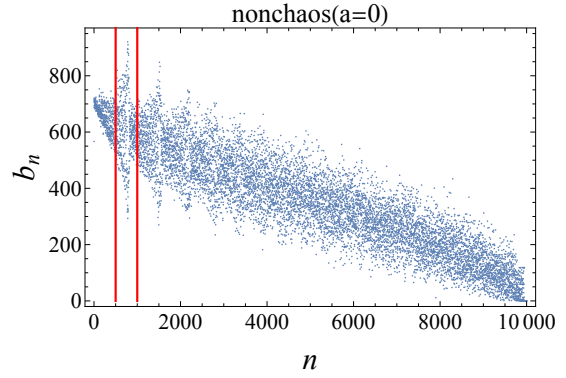
The region Ω is obtained by cutting out a circle of radius l from an equilateral triangle of side length L , as shown in Fig.1. The system is integrable when $l = 0$ and chaotic when $0 < l < L$. For convenient, the area of Ω is kept at 1 and the parameter $a \equiv l/L$ is introduced, whose value determines the degree of chaos for the system.

For practical computation in the energy representation, firstly we set the value \mathcal{N}_{max} to truncate the maximum number of energy levels. Here we adopt the convention $\mathcal{N}_{max} = 100$ in accordance with [11]. Secondly, we pick a random matrix $\mathcal{M}_{\mathcal{O}}$ of size 100×100 from the probability distributions (3.2) and (3.3), which is the matrix of the initial random operator \mathcal{O} . Then we compute the Lanczos coefficient $\{b_n\}$ of $\mathcal{K}_m(\mathcal{L}, \mathcal{M}_{\mathcal{O}})$ by the algorithm in Section 2. To calculate the variance σ^2 of the Lanczos coefficients, we choose $5\mathcal{N}_{max}$ coefficients in consistent with [11]. The set of coefficients $\{b_n\}$ is from the algorithm step sizes $500 \leq n \leq 1000$, as shown in the Fig.2a. Note that this selection of the set of $\{b_n\}$ does not qualitatively affect the result of this paper. The effect of selecting the set of $\{b_n\}$ from different algorithm step sizes is discussed in the appendix B. Finally, we repeat this process 5000 times to get the resulting distribution function $f(\mathcal{O})$.

For the different distributions (GOE, GUE, URE, UIM and UCP) of initial operators, the sampled variances σ^2 are shown in Fig. 3, where m labels the samples. For visual cleanness, we only show 1000 samples instead of all 5000 samples. For GOE and GUE, they overlap completely in the nonchaotic case in Fig. 3b, and separate from each other in the chaotic case in Fig. 3a. Similary for the uniform distributions, they mix together in the nonchaotic case in Fig. 3d, and split into two separated groups in the chaotic case in Fig. 3c, with URE and UIM being one group and UCP being the other.

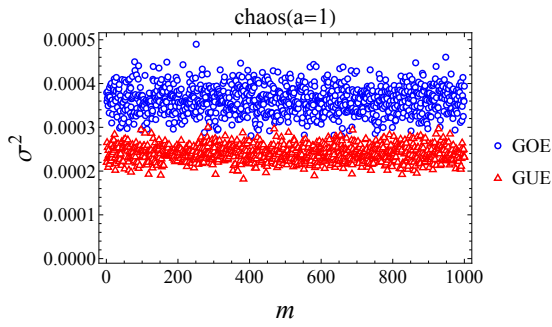


(a) b_n in chaotic case $a = 1$.

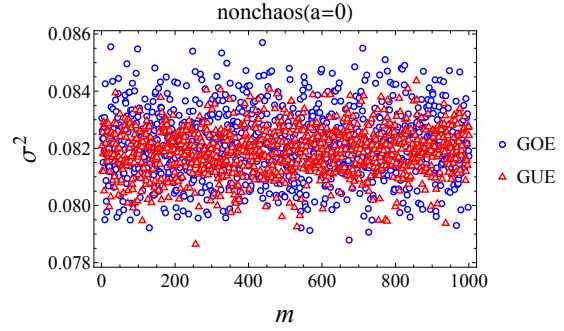


(b) b_n in nonchaotic case $a = 0$.

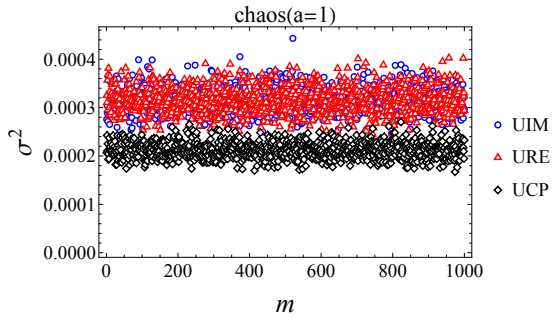
Figure 2: The Lanczos coefficients $\{b_n\}$ for an initial operator selected from GUE. The sets of coefficients between the two red lines ($500 \leq n \leq 1000$) are used to calculate the variance σ^2 (2.7).



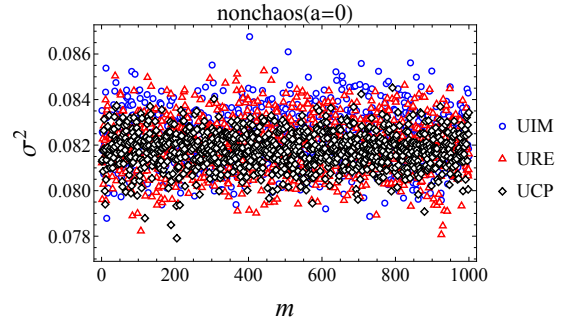
(a) Sampled variances σ^2 of GOE and GUE in chaotic case $a = 1$.



(b) Sampled variances σ^2 of GOE and GUE in nonchaotic case $a = 0$.



(c) Sampled variances σ^2 of uniform distributions in chaotic case $a = 1$.



(d) Sampled variances σ^2 of uniform distributions in nonchaotic case $a = 0$.

Figure 3: Samples of variances σ^2 for GOE, GUE, URE, UIM and UCP. The horizontal axis represents the m th sampling. The chaotic $a = 1$ and nonchaotic case $a = 0$ have different behaviors.

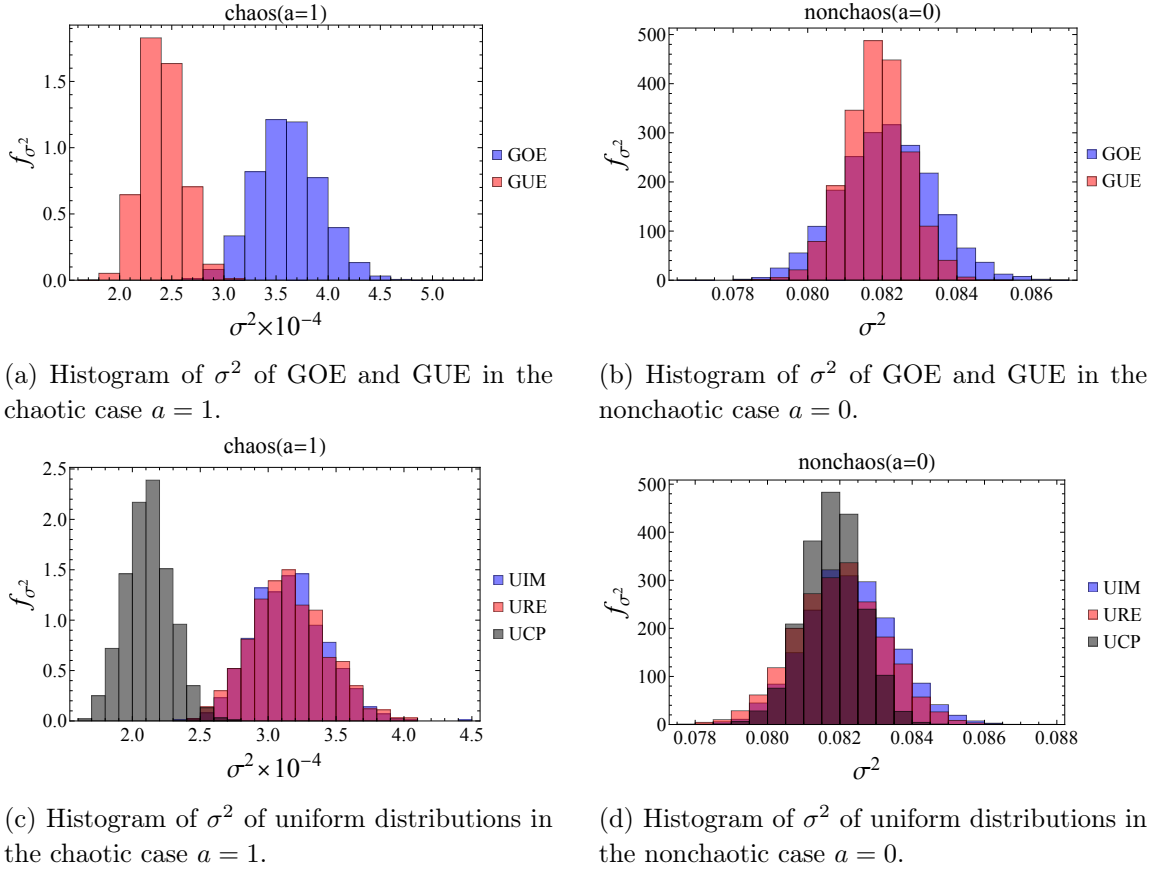


Figure 4: The histogram of variances σ^2 after sampling the initial operator 5000 times from GOE, GUE, URE, UIM and UCP. Obviously they resemble normal distributions.

The corresponding histogram of the sampled σ^2 is shown in Fig. 4, which shows that the resulting probability distribution resembles the normal distribution. For the Gaussian ensembles, we can see clearly that they are overlapped in the nonchaotic case in Fig. 4b and separated in the chaotic case in Fig. 4a. For the uniform distributions, they are overlapped in the nonchaotic case in Fig. 4d. In the chaotic case in Fig. 4c, URE and UIM are still together, but they are separated from UCP.

We have shown the Gaussian ensembles and the uniform distributions separately for visual cleanness in the above figures 3 and 4. Their axis values indicate that they can be compared together in one figure. For this purpose, we fit¹ their histogram to the normal distribution and find the average value $\langle \sigma^2 \rangle$ and the standard deviation, which characterize the resulting distribution f_{σ^2} . Then the resulting distribution f_{σ^2} can be shown in a figure where the point is this average value and the error bar is the standard deviation. For all different distributions (GOE, GUE, URE, UIM and UCP) of initial operators, the resulting distributions f_{σ^2} are shown in Fig. 5, as the system varies from nonchaotic $a = 0$ to chaotic $a = 1$. We see that when the system is nonchaotic, the data points of all distributions

¹The details of this data fitting is shown in the Appendix A.

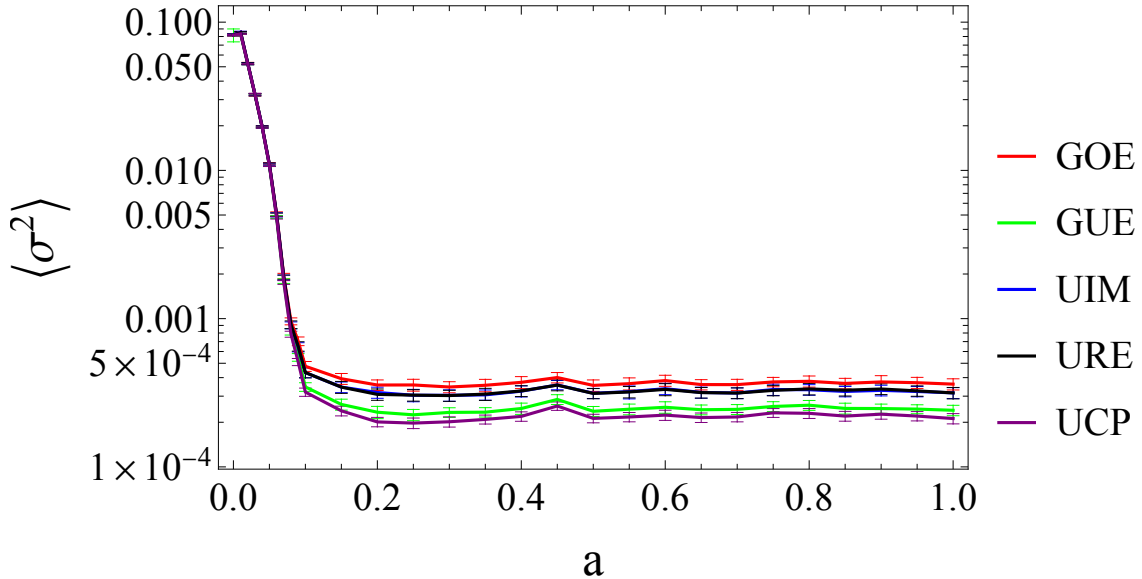


Figure 5: The logarithm plot of the average $\langle \sigma^2 \rangle$ of resulting normal distributions f_{σ^2} , for all different distributions (GOE, GUE, URE, UIM and UCP) of initial operators. The error bar is the standard deviation. The system dynamics changes from nonchaotic to chaotic, as a varies from 0 to 1.

overlap together within the range of error bars. As the system becomes chaotic, different distributions start to separate at $a = 0.1$ and the distance of separation is roughly fixed after $a = 0.15$. Note that the axis is logarithmic, so the separation is very large. We see that they split into two groups well-separated: one group is of GOE, URE and UIM, the other group is GUE and UCP.

6 Discussion

Firstly, we emphasize the importance of the resulting distribution being the normal distribution. We repeat the computation for $\mathcal{N}_{max} = 5$ in Appendix C, where the resulting distribution f_{σ^2} is not normal and there is no separation of f_{σ^2} in the chaotic case. This suggests that the resulting distributions being normal is essential for their separation behavior in the chaotic case.

Qualitatively we can understand this by the central limit theorem as discussed in Section 4. The resulting distribution being normal means that we have enough random numbers in the sample, so that the statistics is reliable and robust. Luckily, the typical choice of $\mathcal{N}_{max} = 100$ in literature is adequate for the normal distribution. It remains an open problem to quantitatively understand the connection between being normal distributions and the separation behavior in the chaotic case.

Secondly, we emphasize that these overlapping-separating behaviors do not depend on the choice of algorithm step-sizes of coefficients $\{b_n\}$. In appendix B, we choose the step-sizes $1000 \leq n \leq 1500$ from the Krylov space in Fig. 2. We still get the resulting normal

distributions and the overlapping-splitting behaviors. Note that the detailed values of the average and the standard deviation will change, it is the overlapping-separating behavior that does not change. It remains an open problem to quantitatively prove this independence on different choices of algorithm step-sizes.

Thirdly, we discuss the resulting two groups of separation. The GOE, URE and UIM are in one group. We can view GOE, URE and UIM as essentially composed of only real numbers, because the UIM is just real numbers multiplied by the overall factor-the imaginary i . The other group is GUE and UCP, which are essentially composed of complex numbers with both real and imaginary parts. So one group is essentially related with one-dimensional random numbers and the other group is related with two-dimensional random numbers. This distinction between real and complex numbers may be related to the nature of the integrability-breaking-term, or to the symmetry of the model. This remains to be one of the open problems.

Finally, for the chaotic case, we compare our separation behavior with a similar behavior-of-separation in RMT [10]. For a spin system [10] under chaotic dynamics, the Hamiltonian is sampled from RMT ensembles while the initial operator is fixed. For Hamiltonians from GUE and GOE, a separation is obtained in the late-time saturation of the Krylov complexity. Qualitatively, the behavior of late-time saturation of K-complexity are consistent with the behavior of variances σ^2 of the Lanczos coefficients [4]. So it might be possible that the ensemble average of the variance σ^2 over RMT Hamiltonian are also separating in [10], although it is not computed there. If this indeed happen, the separation behavior of the resulting distributions f_{σ^2} and of the late-time saturation of the Krylov complexity can be viewed as 'dual' to each other for chaotic systems.

Qualitatively, this 'duality' can be understood as following: in one side, the Hamiltonian are random and the initial operator is fixed, and in the other side, the Hamiltonian is fixed and the initial operators are random. They are 'equivalent' when taking the statistics, at least for chaotic systems. From the proof (4.7) of the lemma in Section 4, we see that the Lanczos coefficients and the Krylov basis depend only on the initial operators and energy levels. Both the random energy levels and random initial operators can give random Lanczos coefficients, so intuitively, these statistics can be viewed as dual or equivalent. It remains an open problem to quantitatively prove this connection.

In conclusion, we pick the Sinai billiard and generate random initial operators from given probability distributions (GOE, GUE, URE, UIM and UCP). Then we find that the resulting distributions of the variance of Lanczos coefficients are normal distributions. They are overlapped in the nonchaotic case. When the system becomes chaotic, they split into two groups, with one group composed of GOE, URE and UIM, and the other group composed of GUE and UCP. We analyze the reason of being normal and discuss the overlap-separation behavior with open problems.

Acknowledgments

Wei Fan is supported in part by the National Natural Science Foundation of China under Grant No. 12105121.

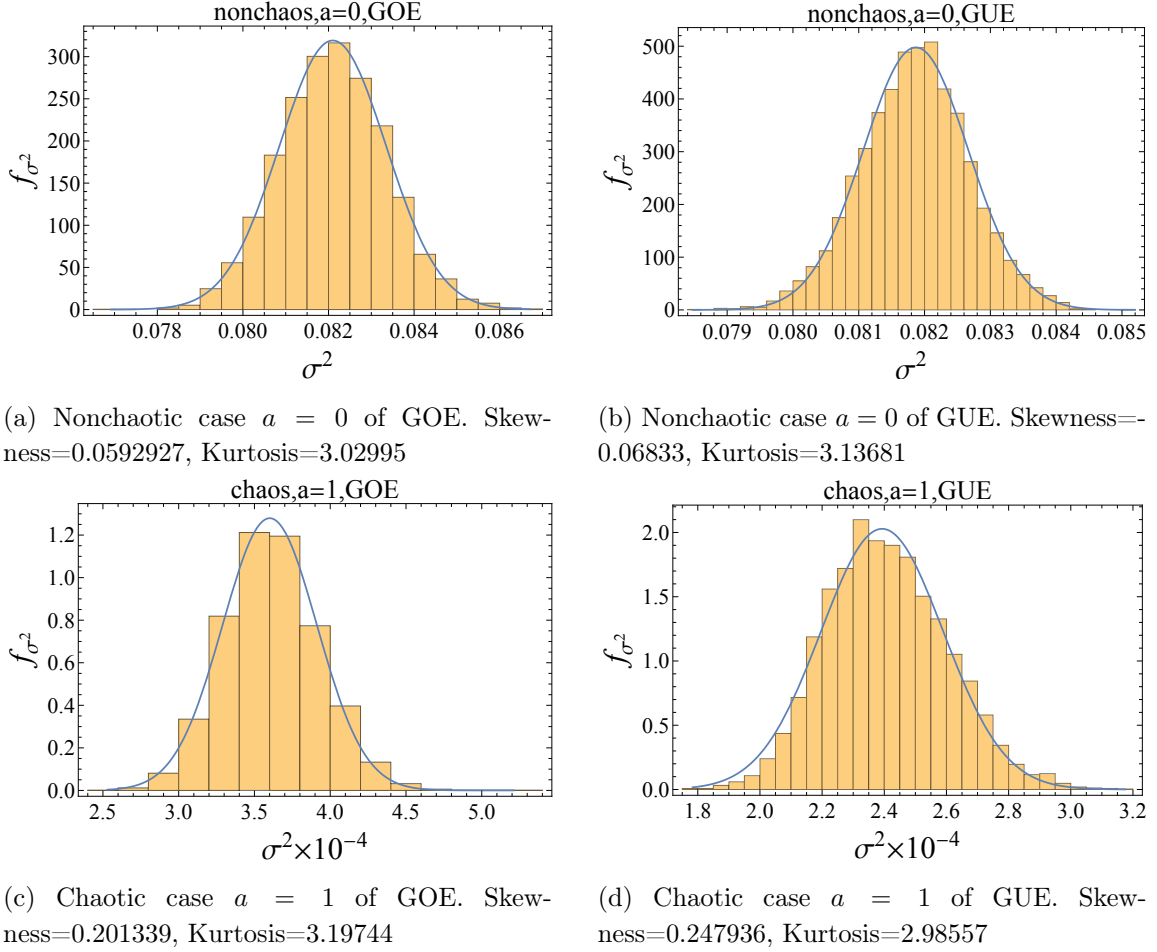


Figure 6: Fitted normal distribution for GOE and GUE, $\mathcal{N}_{max} = 100$.

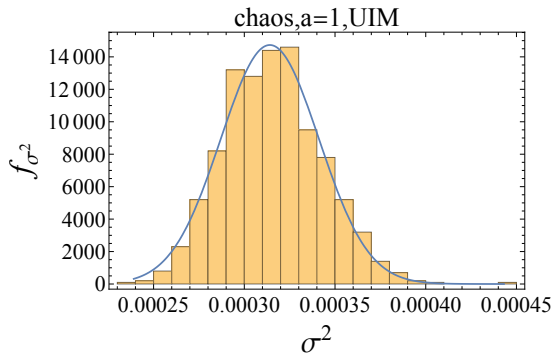
A Check the normal distribution of σ^2 for $\mathcal{N}_{max} = 100$

Here we show the data fitting of the histogram in Fig. 4 to the normal distribution. For GOE and GUE, the fitted distribution is shown in Fig. 6. For uniform distributions, the fitted distribution is shown in Fig. 7. The average value and the standard deviation are listed in Table 1, where we compare the values obtained from the sampled data and from the fitted normal distribution.

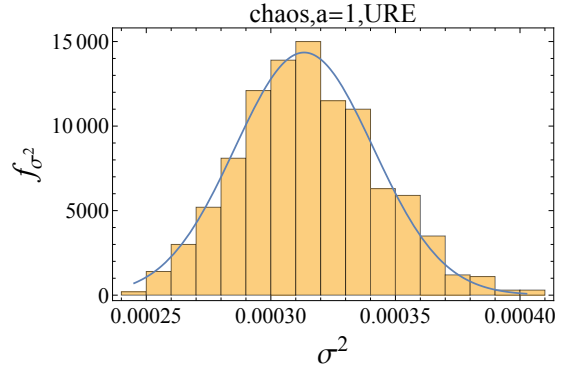
B Different choice of algorithm step sizes for b_n

For the overlapping-separating behavior, here we show its independence on the sets of coefficients used in computing σ^2 . Now we choose the Lanczos coefficients $\{b_n\}$ from step-sizes $1000 \leq n \leq 1500$.

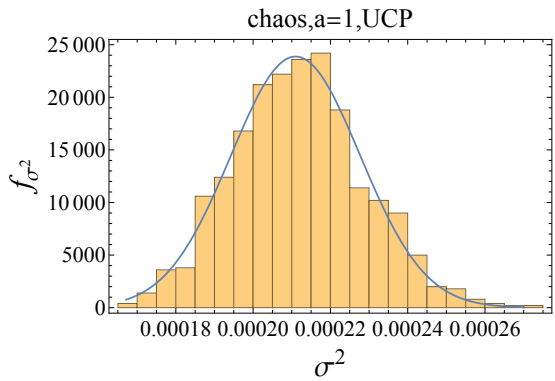
Firstly, we compute the variance σ^2 (2.7) for GOE and GUE, where the first 1000 samples are shown in Fig. 8. We see that GOE and GUE mix together in the nonchaotic case and separate from each other in the chaotic case.



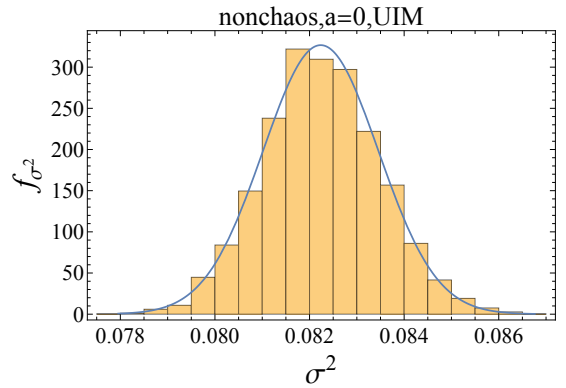
(a) Chaotic case $a = 1$ of UIM. Skewness=0.306957, Kurtosis=3.26486.



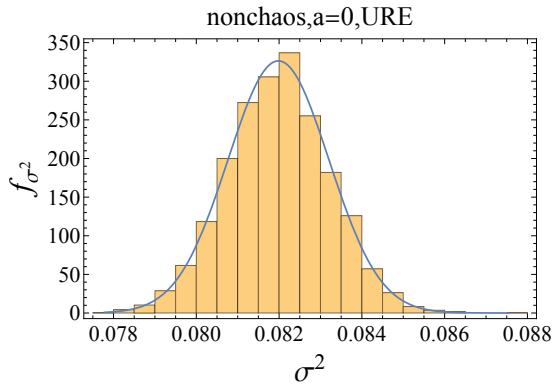
(b) Chaotic case $a = 1$ of URE. Skewness=0.234259, Kurtosis=2.88038.



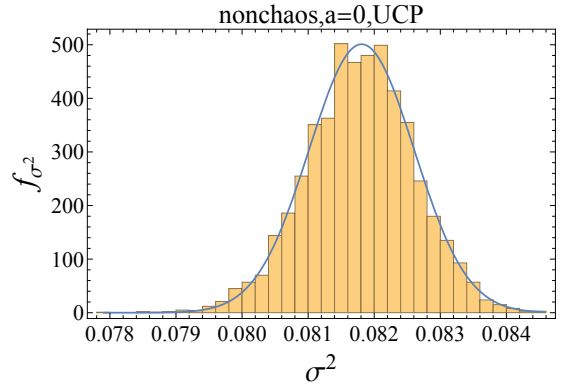
(c) Chaotic case $a = 1$ of UCP. Skewness=0.207669, Kurtosis=2.97609.



(d) Nonchaotic case $a = 0$ of UIM. Skewness=0.0715752, Kurtosis=2.99478.



(e) Nonchaotic case $a = 0$ of URE. Skewness=0.0339498, Kurtosis=3.07535.



(f) Nonchaotic case $a = 0$ of UCP. Skewness=-0.135062, Kurtosis=3.25632.

Figure 7: Fitted normal distribution for uniform distributions, $\mathcal{N}_{max} = 100$.

		$\mathcal{N}_{max} = 100$		
			μ_0	σ_0
nonchaos	GOE	Fit	0.08205	0.00125033
		Data	0.0821079	0.00124627
	GUE	Fit	0.0818423	0.000799776
		Data	0.0818522	0.000818971
	URE	Fit	0.0819847	0.00122253
		Data	0.0819877	0.00122892
	UIM	Fit	0.0822362	0.001221
		Data	0.0822584	0.0012246
	UCP	Fit	0.0818089	0.000796413
		Data	0.0817893	0.000813977
chaos	GOE	Fit	0.000360084	0.0000311866
		Data	0.000361536	0.0000312431
	GUE	Fit	0.000239301	0.0000196699
		Data	0.00024081	0.0000194523
	URE	Fit	0.000313361	0.0000277979
		Data	0.000315455	0.0000278845
	UIM	Fit	0.000314084	0.0000270829
		Data	0.000315694	0.0000267367
	UCP	Fit	0.000210981	0.0000167099
		Data	0.000211866	0.0000168488

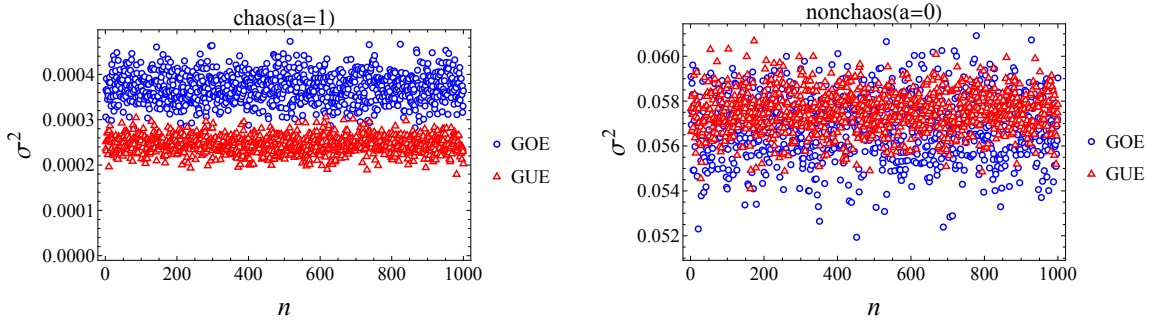
Table 1: Average μ_0 and standard deviation σ_0 for the data fitting, $\mathcal{N}_{max} = 100$. 'Data' means the values computed from the sampled data. 'Fit' means the values of the fitted normal distribution.

Then, the histogram of all 5000 samples are shown in Fig. 9. Obviously they still resemble normal distributions and are overlapped in the nonchaotic case and well-separated in the chaotic case.

Finally, the fitted normal distributions are shown in Fig. 10. So we still get the resulting normal distributions and the overlapping-splitting behaviors, although the detailed values of the average and the standard deviation change.

C Check the normal distribution of σ^2 for $\mathcal{N}_{max} = 5$

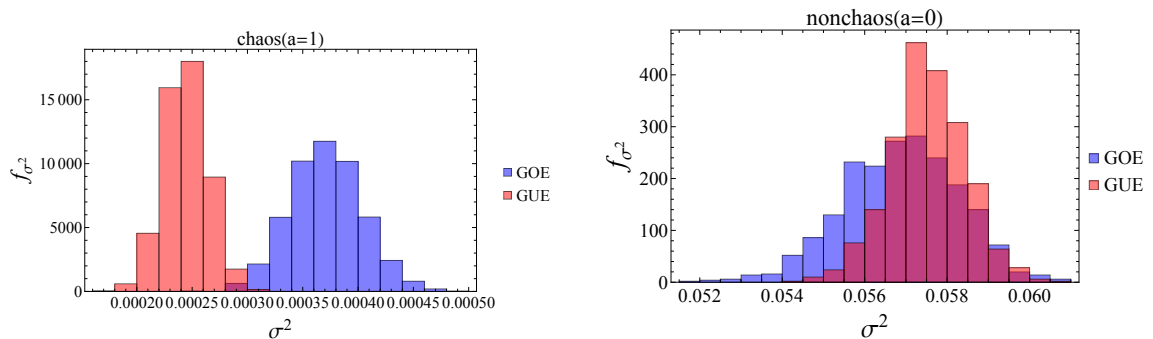
Here we study the case of $\mathcal{N}_{max} = 5$. Then the sets of coefficients b_n are chosen from step-sizes $1 < n < 15$. We repeat the computation for GOE and GUE, and show that there



(a) Sampled variances σ^2 of GOE and GUE in chaotic case $a = 1$.

(b) Sampled variances σ^2 of GOE and GUE in nonchaotic case $a = 0$.

Figure 8: The first 1000 samples of variances σ^2 for GOE and GUE. Here the Lanczos coefficients $\{b_n\}$ from step-sizes $1000 \leq n \leq 1500$ are used.



(a) Histogram of σ^2 of GOE and GUE in the chaotic case $a = 1$.

(b) Histogram of σ^2 of GOE and GUE in the nonchaotic case $a = 0$.

Figure 9: The histogram of variances σ^2 after sampling the initial operator 5000 times from GOE and GUE. The Lanczos coefficients $\{b_n\}$ from step-sizes $1000 \leq n \leq 1500$ are used. They are overlapped in the nonchaotic case and well-separated in the chaotic case.

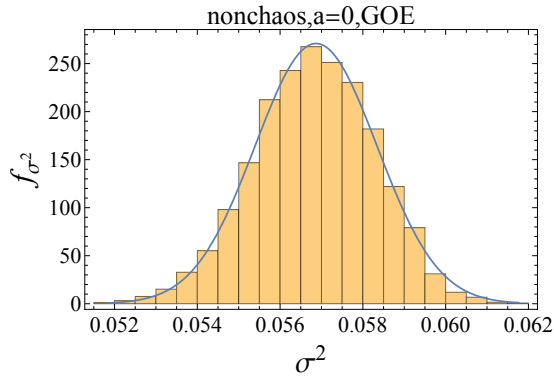
is neither normal distributions nor separating behaviors.

The histogram of all 5000 samples are shown in Fig. 11. Obviously they are not normal distributions and are not separated in the chaotic case.

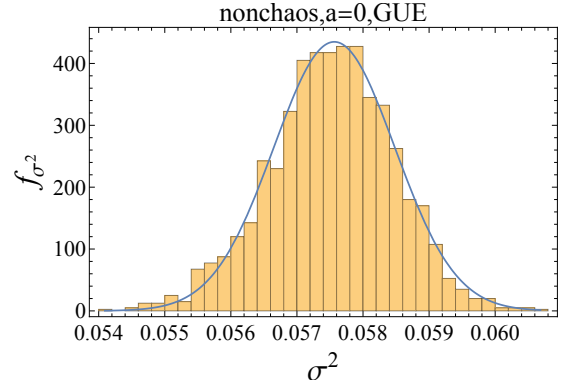
Anyway, if we force to fit the histogram to normal distributions, the results are shown Fig. 12. From the ridiculous value of skewness and kurtosis, we understand that the histogram can not be the normal distribution. Also, from the values listed in Table 2, we see that there is large discrepancy between values from the sample data and values from the fitted distribution. So for $\mathcal{N}_{max} = 5$, the resulting distributions are not normal and there is no separating behaviors between GOE and GUE.

References

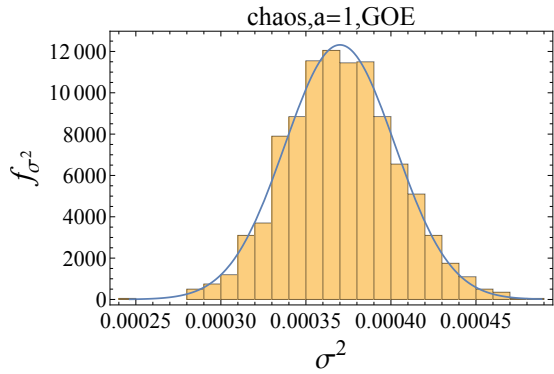
[1] D.E. Parker, X. Cao, A. Avdoshkin, T. Scaffidi and E. Altman, *A Universal Operator Growth Hypothesis*, *Phys. Rev. X* **9** (2019) 041017 [1812.08657].



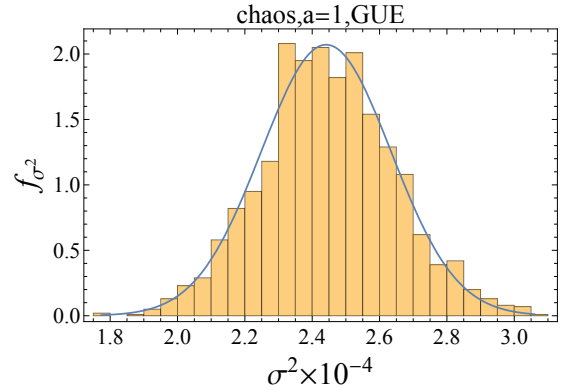
(a) Nonchaotic case $a = 0$ of GOE. Skewness= -0.113535 , Kurtosis= 2.94238 .



(b) Nonchaotic case $a = 0$ of GUE. Skewness= -0.156533 , Kurtosis= 3.16475 .

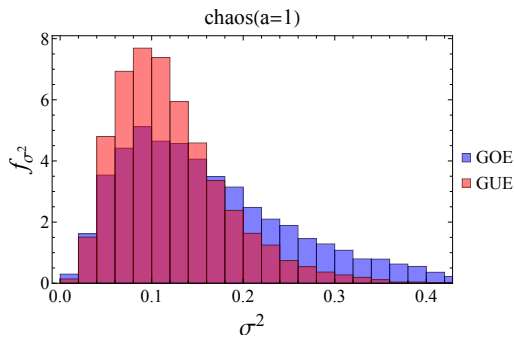


(c) Chaotic case $a = 1$ of GOE. Skewness= 0.107514 , Kurtosis= 3.01354 .

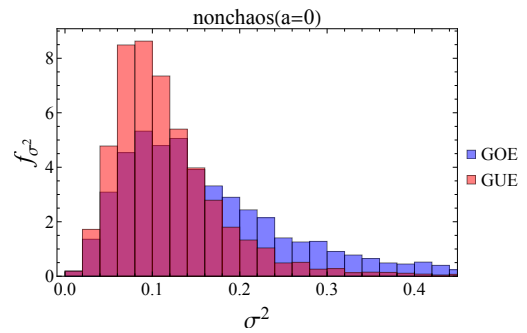


(d) Chaotic case $a = 1$ of GUE. Skewness= 0.0881284 , Kurtosis= 3.06162 .

Figure 10: Fitted normal distribution for GOE and GUE, $\mathcal{N}_{max} = 100$. The Lanczos coefficients $\{b_n\}$ from step-sizes $1000 \leq n \leq 1500$ are used.

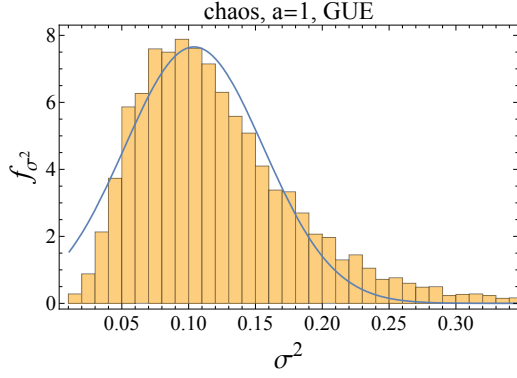


(a) Histogram of σ^2 of GOE and GUE in the chaotic case $a = 1$.

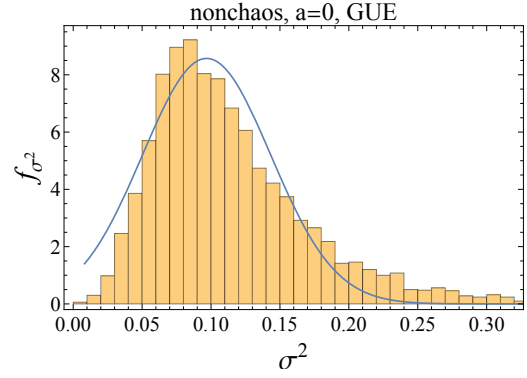


(b) Histogram of σ^2 of GOE and GUE in the nonchaotic case $a = 0$.

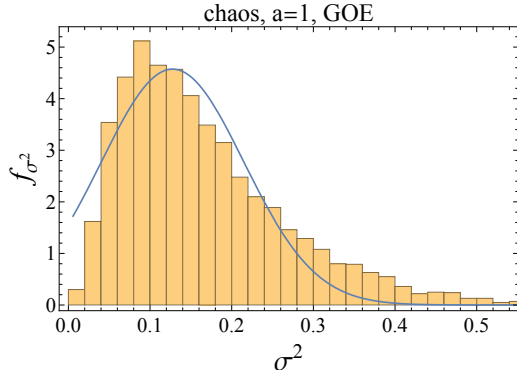
Figure 11: The histogram of variances σ^2 after sampling the initial operator 5000 times from GOE and GUE, $\mathcal{N}_{max} = 5$. Obviously they are not normal distributions.



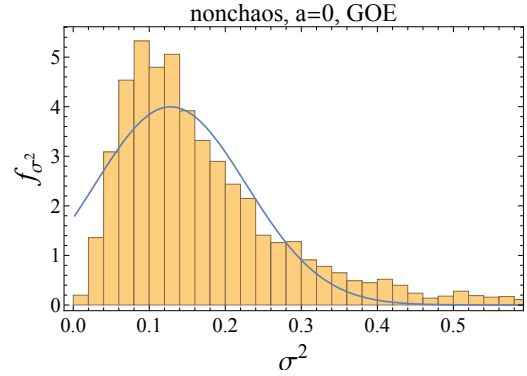
(a) $N = 5$ chaos, Gaussian U ensembles. Skewness=1.19843, Kurtosis=5.18562.



(b) $N = 5$ nonchaos, Gaussian U ensembles. Skewness=4.30801, Kurtosis=50.7359.



(c) $N = 5$ chaos, Gaussian O ensembles. Skewness=1.6231, Kurtosis=7.05429.



(d) $N = 5$ nonchaos, Gaussian O ensembles. Skewness=5.83862, Kurtosis=73.6201.

Figure 12: Data fitting for GOE and GUE, $\mathcal{N}_{max} = 5$. The large value of skewness and kurtosis means that they can not be normal.

- [2] J. Maldacena, S.H. Shenker and D. Stanford, *A bound on chaos*, *JHEP* **08** (2016) 106 [[1503.01409](#)].
- [3] A.I. Larkin and Y.N. Ovchinnikov, *Quasiclassical Method in the Theory of Superconductivity*, *Soviet Journal of Experimental and Theoretical Physics* **28** (1969) 1200.
- [4] E. Rabinovici, A. Sánchez-Garrido, R. Shir and J. Sonner, *Krylov localization and suppression of complexity*, *JHEP* **03** (2022) 211 [[2112.12128](#)].
- [5] F.J. Dyson, *Statistical Theory of the Energy Levels of Complex Systems. II*, *Journal of Mathematical Physics* **3** (1962) 157.
- [6] M.C. Gutzwiller, *Periodic orbits and classical quantization conditions*, *J. Math. Phys.* **12** (1971) 343.
- [7] M.V. Berry and M. Tabor, *Level Clustering in the Regular Spectrum*, *Proceedings of the Royal Society of London Series A* **356** (1977) 375.
- [8] O. Bohigas, M.J. Giannoni and C. Schmit, *Characterization of chaotic quantum spectra and universality of level fluctuation laws*, *Phys. Rev. Lett.* **52** (1984) 1.

		$\mathcal{N}_{max} = 5$		
		μ_0	σ_0	
nonchaos	GOE	Fit	0.128068	0.099812
		Data	0.188669	0.178039
	GUE	Fit	0.0967919	0.0465464
		Data	0.119184	0.0752851
	URE	Fit	0.119756	0.0814372
		Data	0.169944	0.146747
	UIM	Fit	0.206881	0.220034
		Data	0.467013	0.602757
	UCP	Fit	0.0678911	0.0397609
		Data	0.0877107	0.0616032
chaos	GOE	Fit	0.127619	0.0872543
		Data	0.170123	0.112041
	GUE	Fit	0.104014	0.0521167
		Data	0.121707	0.0610372
	URE	Fit	0.112995	0.0772997
		Data	0.150244	0.0991289
	UIM	Fit	0.20724	0.0973048
		Data	0.253492	0.14551
	UCP	Fit	0.0688293	0.0407356
		Data	0.0853616	0.0509862

Table 2: Average μ_0 and standard deviation σ_0 for the data fitting, $\mathcal{N}_{max} = 5$. There is large discrepancy between values computed from the sampled data and values of the fitted normal distribution.

- [9] R. Blümel and U. Smilansky, *Random-matrix description of chaotic scattering: Semiclassical approach*, *prl* **64** (1990) 241.
- [10] E. Rabinovici, A. Sánchez-Garrido, R. Shir and J. Sonner, *Krylov complexity from integrability to chaos*, *JHEP* **07** (2022) 151 [[2207.07701](#)].
- [11] K. Hashimoto, K. Murata, N. Tanahashi and R. Watanabe, *Krylov complexity and chaos in quantum mechanics*, *JHEP* **11** (2023) 040 [[2305.16669](#)].
- [12] B. Craps, O. Evnin and G. Pascuzzi, *Multiseed Krylov complexity*, [2409.15666](#).
- [13] M. Berry, *Quantizing a classically ergodic system: Sinai's billiard and the kkr method*, *Annals of Physics* **131** (1981) 163.
- [14] M. Mehta, *Random Matrices*, Academic Press (1991).